Hindawi
Mobile Information Systems
Volume 2022, Article ID 5344652, 9 pages
https://doi.org/10.1155/2022/5344652

Research Article

Mechanical Fault Diagnosis Technology of Wind Turbine Transmission System Based on Image Features

Lisen Li,[1] **Wenfeng Wang**,[2] **Anmin Cai**,[1] **Hui Li**,[2] **Linwei Zhang**,[1] **and Pengcheng Liu**[2]

[1]*Huaneng Clean Energy Research Institute, Beijing 102209, China*
[2]*Huaneng New Energy Co. Ltd, Shandong Branch, Jinan 250002, Shandong, China*

Correspondence should be addressed to Lisen Li; 120192201158@ncepu.edu.cn

Received 19 May 2022; Revised 15 July 2022; Accepted 22 July 2022; Published 31 August 2022

Academic Editor: Imran Shafique Ansari

China's wind power industry has grown dramatically in recent years as the country's focus on clean energy and renewable energy generation has increased. Mechanical fault diagnosis of wind power transmission is a common wind maintenance method. It has recently become a research hotspot in the field of mechanical fault diagnosis as a method of fault identification based on picture attributes. Time-frequency images, on the other hand, are better for fault analysis and fault diagnosis of wind power transmission machinery than time-domain and frequency-domain images because they contain more information about the operation status of the gear. This work proposes and applies an image feature extraction-based fault diagnostic method to the defect diagnosis of wind-driven mechanical gears. The feature extraction suitable for gear and gear box faults is analyzed, and the improved artificial immune algorithm is used for fault identification. Through collecting normal vibration signals and two kinds of fault vibration signals from the gearbox of wind power transmission in a wind farm and extracting image features on the basis of data processing, the improved algorithm is finally applied for fault analysis. The experimental results show that the fault diagnosis rate of the improved real-value negative selection algorithm is obviously improved and can improve the fault diagnosis rate by 5%.

1. Introduction

Wind power drive systems often operate in harsh working environments, and faults can be detected and diagnosed through signal processing techniques. In the past 30 years, fault diagnosis of rotating motors has attracted a lot of research interest [1]. Reducing maintenance costs and preventing accidental downtime are the primary tasks for manufacturers and operators of electrical drives [2]. Bearing failure is one of the most common causes of rotating machinery failure, hence bearing prediction is critical for increasing availability and lowering costs. The use of a condition monitoring and fault diagnosis system (CMFDS) on wind turbines is crucial for reducing unplanned failures [3, 4]. Fault identification has always been a difficult issue for motor systems; it becomes even more difficult in wind energy conversion systems, because the sustainability and feasibility of wind farms are heavily reliant on lowering operation and maintenance costs [5, 6]. For condition-based maintenance of gear transmission systems, reliable identification of fault types and assessment of fault severity are required as well as diagnosis of mechanical faults of wind power transmission through image feature extraction [7, 8].

Once the transmission mechanism of the wind turbine fails, it will send a signal through the change of the vibration signal. In recent years, the monitoring and diagnosis of mechanical faults are usually realized by monitoring and analyzing their vibration signals. Vibration data, especially those collected during system start-up and stop, contain abundant information about gearbox condition monitoring [9]. When mechanical equipment fails, it is usually reflected in vibration signals. Cheng et al. [10] Villa et al. discovered an adaptive time-frequency analysis method based on local mean decomposition for diagnosing gear and roller bearing problems (LMD). Aiming at the modulation characteristics of fault vibration signal of gear or roller bearing, an LMD-based defect detection method for rotating equipment is proposed, which can effectively detect equipment operating

failures [11] and uses the vibration information of the mechanical system under various loads and velocities to predict and detect faults, which is faster and more reliable than the analysis under limited working conditions. Multicomponent extraction is a feasible method for analyzing vibration signals of rotating machinery. Therefore, Wang et al. [12] Raj and Murali designed a friction defect diagnosis method (VMD) based on variational mode decomposition. Bearing faults in rotating machinery are usually regarded as vibration signal pulses [13]. This paper proposes a new morphological algorithm and a fuzzy inference technique to eliminate noise and detect pulses. Muralidharan and Sugumaran [14] use three methods, feature extraction, classification, and classification comparison to implement the vibration-based integrated centrifugal pump condition monitoring system, to improve the inspection efficiency of rotating machinery. The wavelet analysis of feature extraction and NaveBayes algorithm and Bayes network classification algorithm are compared.

For wind power transmission machinery, time-frequency image contains abundant operation status information, which is more suitable for fault analysis of wind power transmission machinery. Younus and Yang [15] propose a new intelligent diagnosis system, that features a selection of tools based on Mahalanobis distance and a relief algorithm which is used to select significant features that can represent machine conditions to improve classification accuracy [16]. For rotating machinery, an improved multiwavelet packet EEMD multifault diagnosis approach was proposed. To improve EEMD decomposition findings and boost weak multifault feature components in distinct narrow bands, a multi-wavelet packet is utilized as a prefilter. By selecting an appropriate increase in noise amplitude based on the vibration characteristics, the EEMD is further improved to improve the accuracy and validity of the decomposition results. In rotating machinery fault diagnosis, Yan et al. [17] summarized fault diagnosis based on continuous wavelet transform, fault diagnosis based on discrete wavelet transform, fault diagnosis based on wavelet packet transform, and fault diagnosis based on second-generation wavelet transform. Tobon-Mejia et al. [18] provide a new approach for estimating the residual service life and bearing confidence based on wavelet packet decomposition and Gauss mixture hidden Markov model. He et al. [19] propose a set of super-wavelet transforms (ESW) to examine the vibration characteristics of motor bearing failures, in order to realize the flexibility of fault features, based on a combination of tunable Q-factor wavelet transform (TQWT) and Hilbert transform. The use of blind source separation (BSS) and nonlinear feature extraction techniques to detect gear box faults is presented. To deal with nonstationary vibration and retrieve the original fault eigenvector, Li et al. [20] employ the wavelet packet transform (WPT) and empirical mode decomposition (EMD) nonlinear analytic methods, capable of stable and accurate analysis of gear failures.

The fault diagnosis method based on artificial neural network can process and accept vague information, and has the ability of self-learning and self-organization. It has high nonlinearity, high fault tolerance, and parallel processing. These characteristics make it well applied in the field of fault diagnosis and get good results. In order to process massive fault data in time and provide accurate diagnostic results automatically, there are scholars who have done a lot of research on intelligent fault diagnosis of rotating machinery and proposed a diagnosis method based on deep neural network, which uses signal processing technology to extract features and input them into ANN to classify faults. The diagnostic findings reveal that this method not only adapts to the available fault features in the measured signals but also has higher diagnostic accuracy than previous methods. Scholars proposed a new method based on wavelet packet decomposition (WPD) and empirical mode decomposition (EMD), which extracted the fault characteristic frequency of rotating machinery and the early fault diagnosis method of neural network, based on an analysis of the shortcomings of current feature extraction and fault diagnosis techniques. A rotating equipment fault diagnosis model with transverse early cracks is investigated. The results suggest that this method can effectively acquire signal characteristics in order to diagnose rotating machinery early faults. Scholars have developed a mathematical study for determining the most significant intrinsic mode function (IMF). To classify bearing defects, the selected features were used to train an artificial neural network (ANN). The experimental findings suggest that the proposed method for classifying bearing faults based on vibration signals of operation failure is accurate, the accuracy of fault classification can reach 98%. To extract universal multiclass pavement statistical characteristics, researchers suggested a new intelligent problem detection scheme based on wavelet packet transform (WPT), distance assessment technology (DET), and support vector regression (SVR). WPT preprocesses the gathered signals at various decomposition depths. Scholars have used the K-nearest neighbor (KNN) classifier to determine the condition of a ball bearing using vibration and load signals.

This research investigates a defect diagnosis approach for wind turbine transmission machinery based on picture feature extraction, to improve the detection of wind power transmission mechanical faults. That is, vibration signals from important components of the wind turbine transmission system, such as the gearbox, low-speed spindle, high-speed shaft, and generator, are gathered in both normal and fault modes. Time-frequency analysis employing short-time Fourier transform and wavelet transform yields the time-frequency spectrum. The time-frequency image features are then extracted using a gray level co-occurrence matrix, and the feature vectors are obtained using an artificial immune algorithm for fault diagnosis, resulting in improved fault diagnosis accuracy.

2. Proposed Method

The general process of fault diagnosis of wind power transmission machinery based on image features includes image acquisition, image processing, feature extraction, judgment and recognition, and finally early warning or alarm. The overall process is shown in Figure 1. In this paper, the vibration signal processing, feature extraction, judgment, and recognition are studied.

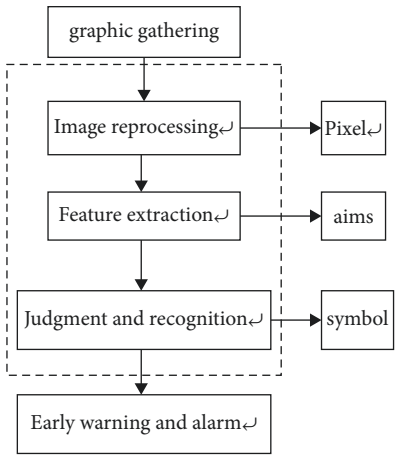

Figure 1: System flow chart.

2.1. Vibration Signal Processing. Vibration signals generated by the mechanical components in the transmission system of wind turbines contain a lot of information related to their mechanical state. However, due to the complex structure and disturbance of wind turbines, and the very unstable operating conditions under the influence of variable wind speeds, the vibration signals show obvious nonstationarity, which makes it difficult to extract the characteristic information of mechanical state. Therefore, the vibration signals of transmission system need to be preprocessed. In addition, due to the interference of strong background noise, its vibration characteristics are easily concealed, so time-frequency analysis method is generally used to process the vibration signal of wind turbine transmission system.

The principle of time-frequency analysis is that the frequency description is given at a given time point, and the frequency description of each time point is given along with the movement of the time axis. From this, a time-frequency joint distribution with horizontal axis as time and vertical axis as frequency is formed, which can accurately diagnose wind power transmission faults through data.

2.1.1. Short-Time Fourier Transform. The basic idea of STFT is that the original signal is truncated by the translation of window function, the nonstationary signal is approximated to some stationary signals by the truncation of signal, and the stationary signals are transformed by Fourier transform to obtain the spectrum of the signal in different time periods. Because of the need for windowed truncation of nonstationary signals, short-time Fourier transform (STFT) is also called windowed Fourier transform (WFT). If the basis function, $g_{t\Omega}(\tau) = g(\tau - t)e^{i\Omega\tau}$, is used, it is defined as:

$$\begin{aligned} \mathrm{STFT}_x(x,\Omega) &= \int_{-\infty}^{\infty} x(\tau)g^*(\tau - t)e^{-i\Omega\tau}\mathrm{d}\tau \\ &= \langle x(\tau), g(\tau - t))e^{i\Omega\tau} \rangle. \end{aligned} \tag{1}$$

In formula, $g(\tau) = 1, g_{t\Omega}(\tau) = 1, \Omega = 2\pi f$, the window function $g(\tau)$ should be a symmetric real function.

For a given time t, $\mathrm{STFT}_x(x,\Omega)$, it is the localization frequency of signal $x(t)$ in a very small range near time t. With the translation of t, all localized spectral features of the whole signal are extracted. Therefore, short-time Fourier transform (STFT) is a bridge between global and local features. From formula 1, the time-shift and frequency-shift characteristics of short-time Fourier transform can be proved.

(1) Time-shift characteristics: STFT does not have time-shift invariance, its amplitude is invariant and its phase difference is a phase factor, see formula.

$$\begin{aligned} &\text{If } y(t) = x(t - t_0), \text{ then } \mathrm{STFT}_y(x,\Omega) \\ &\quad = \mathrm{STFT}_x(t - t_0, \Omega)e^{-i\Omega t_0}. \end{aligned} \tag{2}$$

(2) Frequency shift characteristics: that is, STFT transform keeps the frequency shift of signal (t), see formula.

$$\text{If } y(t) = x(t)e^{it\Omega_0}, \text{ then } \mathrm{STFT}_y(t,\Omega) = \mathrm{STFT}_x(t,\Omega - \Omega_0). \tag{3}$$

In formula (3), $x(t)$ represents the vibration signal.

2.1.2. Wavelet Transform. Its window function can change dynamically with frequency, so it can fully observe the characteristics of the signal and transform the fault signal locally in the time-frequency domain. It can extract the effective information of the fault signal from the signal. It can divide the fault signal into different levels of a multiscale, and has strong scaling and translation functions. At the same time, wavelet transform combines the idea of localization of Fourier transform, and overcomes the problem that window size cannot be transformed freely, so that the window can adjust itself with different frequencies.

Let x(t) be a finite energy function, namely, $x(t) \in L^2(R)$, then its wavelet transform is:

$$w_x(a,b;\varphi) = \int_{-\infty}^{\infty} x(t)\varphi_{a,b}(t)\mathrm{dt},\ a > 0. \tag{4}$$

In formula (4), w represents the result of wavelet transform.

$\varphi_{a,b}(t)$, the basic wavelet function $\varphi(t)$ is translated and scaled to obtain:

$$\varphi_{a,b}(t) = a^{-(1/2)}\varphi\left(\frac{t - b}{a}\right), \tag{5}$$

where b is the location parameter, a >0 is the scale parameter, and $a^{-(1/2)}$ factor is the normalized constant, so that the energy remains unchanged before and after the transformation, that is,

$$\varphi_{a,b}(t)^2 = \int_{-\infty}^{\infty} \left|\varphi_{a,b}(t)\right|^2 \mathrm{d}t = \int_{-\infty}^{\infty} |\varphi(t)|^2 \mathrm{d}t. \quad (6)$$

The frequency domain representation of the wavelet function is as follows:

$$\widehat{\varphi}_{a,b}(\omega) = \sqrt{a} e^{-i\omega} \widehat{\varphi}(a\omega). \quad (7)$$

Formula (7) shows that when the scale parameters become smaller and the time domain resolution becomes higher, the corresponding frequency domain resolution becomes lower; when the scale parameters become larger and the frequency domain resolution becomes higher, the corresponding time domain resolution becomes lower. It shows that the wavelet transform has the advantage of adaptive window. Compared with STFT, the "window function" of wavelet transform is composed of decaying functions, not superimposed triangular functions. Therefore, the wavelet can be scaled adaptively, which solves the problem that the time and frequency resolution cannot reach the optimum at the same time.

2.2. Image Feature Extraction. After the original signal is decomposed by signal processing method, fault features need to be extracted from the scores. If the extracted features can accurately describe the mechanical state of each component of the wind turbine transmission system and have high sensitivity to the change of the mechanical state under different working conditions, the fault identification ability of the fault diagnosis system will be greatly improved.

The quality of feature extraction from time-frequency images will directly affect the fault diagnosis results of wind turbines, so how to extract image feature information has become a research hotspot. Useful information is extracted from the image to describe the rich feature information contained in the two-dimensional image when the wind turbine transmission machinery is normal and faulty.

(1) Image texture feature: It is a measure of the relationship between the pixels in a local area. It includes the arrangement and organization order of the image surface structure. It refers to the surface properties of the information contained in a region of the image, and expresses the change in the gray level of the image pixels in space. In pattern recognition, the texture features of the image can reflect the regional characteristics of the image, can resist the influence of noise and have rotation invariance, and will not cause recognition failure due to errors in some pixels. There are four types of the most commonly used texture feature extraction methods: structural, statistical, spectral, and model.

(2) Usually, the color feature is the feature integration of the pixels in the image or image area, which is based on the image pixels. But the color feature cannot capture the local features of the object in the image, and cannot reflect the change in the size and direction of the image. Common methods of extracting color features are: color histogram and color set, color moment.

(3) Image shape features: Generally, image shape features can be represented by region features or boundary features, which are also widely used in image recognition and other applications.

It is an important method to extract gray level co-occurrence matrix for image texture feature analysis.

2.3. Gray Level Co-Occurrence Matrix. Extracting gray level co-occurrence matrix for image texture feature analysis is an important method for image feature extraction. By studying the joint distribution probability of two different gray level pixels in the image area, it can accurately reflect the spatial complexity, roughness, and repetitive direction of the texture of time-frequency image of wind turbine transmission machinery. Its essence is to start from the pixel (position is (x, y)) whose gray level is i. The frequency $p(i, j, d, \theta)$ of simultaneous occurrence of pixels with distance d and gray level j (position $(x + \Delta x, y + \Delta y)$) is counted.

$$\mathrm{p}(i, j, d, \theta) = |[(x, y), (x + \Delta x, y + \Delta y)| f(x, y) = i; f(x + \Delta x, y + \Delta y) = j]|. \quad (8)$$

In Equation (8), p represents the frequency of simultaneous occurrence of pixels.

In formula, $x, y = 0, 1, 2, \ldots, N - 1$ is the pixel coordinates of the image. $i, j = 0, 1, \ldots L - 1$ is the gray value. $d = (\Delta x, \Delta y)$ is the generation step of GLCM, θ is the direction of GLCM generation, as shown in Figure 2. $\Delta x = d\cos\theta, \Delta = d\sin\theta$, when d and θ is set, we can get an $L * L$ dimension GLCM, which is represented by the symbol P. Generally, the image can be counted in four different directions: 0, 45, 90, and 135.

GLCM can describe the comprehensive information of gray image about direction, adjacent interval, and change range. The characteristic parameters of gray level co-occurrence matrix can be used for texture analysis of gray image.

(1) Contrast (defined as w_1): Used to describe image texture clarity. The bigger the w_1 is, the more obvious the gray difference between adjacent pixel pairs is, and the clearer the image texture is $\mathrm{w}_1 = \sum_{i=1}^{g} \sum_{j=1}^{g} (i - j) p^2(i, j, d, \theta)$

(2) Relevance (defined as w_2): Used to describe the texture direction of an image. The direction of w_2 is the texture direction of an image. It is used to measure the similarity of elements in GLCM in row or column directions.

$$w_2 = \frac{\sum_{i=1}^{g} \sum_{j=1}^{g} \left(i * j * p(, j, d, \theta) - j - \mu_1 * \mu_2\right)}{\sigma_1 * \sigma_2}. \quad (9)$$

In the formula, the mean and standard deviation of μ_1, μ_2 and σ_1, σ_2 are p_1 and p_2, respectively:

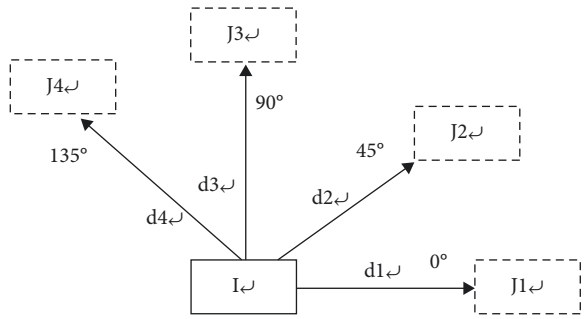

Figure 2: Four generation directions of GLCM.

$$p_1 = \left\{ p_1(i) | p_1(i) = \sum_{j=1}^{g} p(i,j) \right\},$$
$$p_2 = \left\{ p_2(i) | p(i) = \sum_{j=1}^{g} p(i,j) \right\}. \quad (10)$$

(3) Energy (defined as w_3): Also known as angular second-order moment and uniformity, is a measure of image texture uniformity. The larger the w_3, the rougher the image texture is, on the contrary, the finer the texture. When the gray level distribution has a constant or periodic form, the energy reaches its maximum.

$$w_3 = \sum_{i=1}^{g} \sum_{j=1}^{g} p^2(i,j,d,\theta). \quad (11)$$

(4) Inverse Gap (defined as w_4): Measures the local change of image texture. w_4 means that the image contains texture with ideal repetitive structure, so the larger the inverse gap, the more regular the texture.

$$w_4 = \sum_{i=1}^{g} \sum_{j=1}^{g} \frac{p(i,j,d,\theta)}{\left[1 + (i-j)^2\right]}. \quad (12)$$

(5) Entropy (defined as w_5): The complexity of image texture is a measure of the randomness of image content. The larger the w_5 value, the more complex the image is.

$$w_5 = -\sum_{i=1}^{g} \sum_{j=1}^{g} p(i,j,d,\theta) lg p(i,j,d,\theta). \quad (13)$$

(6) Variance: Defined as w_6, $w_6 = \sum\sum (i-m)^2 p(i,j,d,\theta)$

(7) Means(defined as w_7): $w_7 = \sum_{k=2}^{2g} k * P_x(k)$, in formula, $P_x(k) = \sum_{i=1}^{g} \sum_{j=1}^{g} p(i,j,d,\theta)$, $k = 2,3,\ldots,2g$

(8) Variance sum (defined as w_8):

$$w_8 = \sum_{k=2}^{2g} (k - w_7)^2 P_x(k). \quad (14)$$

(9) Variance of difference (defined as w_9): $w_9 = \sum_{k=0}^{g} [k — \sum_{k=0}^{g-1} k * P_y(k)]^2 * P_y(k)$

(10) Sum entropy (defined as w_{10}):

$$w_{10} = -\sum_{k=2}^{2g} P_x(k) * \lg(P_x(k)). \quad (15)$$

(11) Differential entropy (defined as w_{11}): $w_{11} = -\sum_{k=0}^{g-1} P_y(k) * \lg(P_y(k))$

(12) Cluster shadow (defined as w_{12}):

$$w_{12} = -\sum_{i=1}^{g} \sum_{j=1}^{g} \left[(i-u_1) + (j+u_2)\right]^2 * p(i,j,d,\theta). \quad (16)$$

(13) Significant clustering (defined as w_{13}):

$$w_{13} = -\sum_{i=1}^{g} \sum_{j=1}^{g} \left[(i-u_1) + (j+u_2)\right]^4 * p(i,j,d,\theta) \quad (17)$$

(14) Maximum probability (defined as w_{14}):

$$w_{14} = \max_{i,j} (p(i,j,d,\theta)) \quad (18)$$

2.4. Texture Feature Extraction of Time-Frequency Image. There are 14 texture feature parameters calculated by GLCM, but these parameters are not all irrelevant. Therefore, if all the parameters are extracted as features, there will be some redundancy. According to the theoretical analysis and experimental results of texture features of time-frequency image of wind turbine transmission machinery vibration signal, four features are selected in this paper, contrast correlation, energy, and inverse difference, to form texture feature vectors of gray image, and texture analysis is carried out.

$$t = [w_1, w_2, w_3, w_4]. \quad (19)$$

The meanings and ranges of the four eigenvalues are shown in Table 1.

In this paper, we use the gray level co-occurrence matrix based on correlation analysis and Hu invariant moments to fuse the features and read the HU invariant moments of seven Gaussian normalized time-frequency images of the target. Seven invariants defined by u_{pq} under translation, scaling, and rotation transformations, $\varnothing = \{\varnothing_i | i = 1,2,\ldots,7\}$. Four eigenvalues are proposed as feature vectors to fuse gray level co-occurrence matrix to get more obvious eigenvalues.

2.5. Negative Selection Algorithm Based on Improved Dynamic Adjustment of Radius Size. Artificial immune algorithm can train detector and generate detector database. Antigens are matched with mature detector databases to identify antigens and output fault results. The immune network can well describe the relevant characteristics of the immune system through the model of immune molecules, and its role comes from the interaction between immune molecules. Negative

Table 1: Statistical feature description.

Attributes	Description
w_1 (CON(Contrast))	It reflects the total amount of local gray changes in the image, and describes the strength and clarity of the image texture. Range of values [0,(size(GLCM,1)-1)^2] for monochrome images, the value is 0
w_2 (CORRE(Correlation))	By reflecting the linear correlation of the gray level in the image, the extension of one gray value in one direction can be obtained. Range of values [−1,1]
w_3 (ASM(Energy))	The texture thickness and uniformity of the gray level distribution in the image are described by the sum of the squares of all the elements in the gray level co-occurrence matrix. [0,1] range of values the larger the value, the simpler the image texture is
w_4 (IDM(Homogeneity))	Reflect a local texture transformation in the image. The range of values is [0,1]. The larger the value, the slower the texture change between different regions

selection algorithm (NSA) is an important way to train detectors in artificial immune algorithm. The flow chart of the algorithm is shown in Figure 3.

(1) Define a self-sample string S consisting of N characters for the training of detectors.

(2) Initialization detector is generated randomly and matched with self-sample string S. If matched, random generation detector is generated again; if not, it is added to detector set R. This is the negative choice.

(3) Check whether the number of detectors meets the requirement, and return (2) if the number of detectors is not reached; if the number of detectors is reached, it ends.

Aiming at the wide application of eigenvector in the algorithm, the concept of detector is generalized. A real-valued vector detector is proposed. The eigenvectors in real-valued vector detectors must have the same dimension as the eigenvectors in the device's normal state (its own space Ny). And the unique eigenvectors (nonself-space) of various fault states of wind turbine transmission machinery can only match other eigenvectors in self-space. It cannot match the feature vectors in the normal state, that is, the feature vectors in its own space. Vector detectors satisfy the following formula: E (m, s) > r.

The Euclidean distance is E; the normal state vector in one's own space is s; the detector threshold is r; and the detector vector is m. The larger radius detector reduces the number of detectors, reduces the training time and the detection time. At the same time, small radius detectors are used to cover areas that fixed radius detectors cannot cover, which reduces black holes and improves the coverage of nonself-areas. The process of generating detectors by negative selection algorithm with variable radius is as follows: (Algorithm 1)

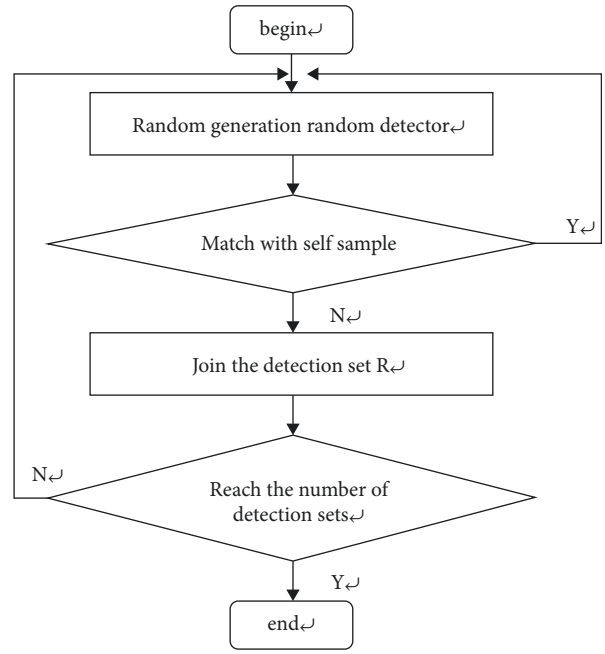

Figure 3: The negative selection algorithm flow chart.

3. Experiments

3.1. Data Source and Processing Flow. The data studied in this paper mainly come from the fault data of large wind turbines in a wind farm. Fan model: SL77-1500; gearbox model: PPSC1290; rated wind speed: 10.8 m/s; single sampling time: 1 min; transmission ratio: 104.125; real-time data monitoring of gears and gearboxes in operation, through fault diagnosis model, the running status of gears and gearboxes is diagnosed. The main types of faults studied in this paper are gearbox broken teeth fault and tooth surface wear and peeling fault.

The vibration signals of gearbox collected by sensors are analyzed, processed, and identified.

3.2. Data Acquisition and Normalization. The experimental data of vibration signals collected by four sensors mainly include three states: normal state, gear broken state, and tooth surface wear state. The mean square eigenvalue was extracted by MATLAB, and 60 groups of normal state data, 10 groups of gear broken state data, and 10 groups of gear surface wear state data were obtained.

3.3. Generating Detector Database by Artificial Immune Algorithms. Artificial immune algorithm is used to train detector and generate detector database. Antigens are matched with mature detector databases to identify antigens and output fault results.

Step 1: D is the empty detector
Step 2: Repeat
Step 3: $t \leftarrow 0, T \leftarrow i, r \leftarrow \infty$
Step 4: Initialize random generation X in normalized real space
Step 5: Repeat, D (i) for each existence
Step 6: Calculate the Euclidean distance between X and detector D (i)
Step 7: If $d < r$(D(i))then t ← t + 1
Step 8: If $t \geq 1/(1 - c_0)$ then Return D else go to 4
Step 9: Each element in Repeat Self-Set S
Step 10: Calculate the distance d1 between X and the elements in self-set S
Step 11: If $dl - r_{self}$ then $r \leftarrow dl - r_{self}$ else $t \leftarrow t + 1$
Step 12: If $t > 1/(1\text{-c})$, C is the maximum coverage of the self, exit
Step 13: Until = m Return D

Algorithm 1: (Self-sample set is S, self-radius is rself , number of detectors is $8\,m$; nonself-coverage rate is c0).

Table 2: The self-sample data.

Mean square dataset				Normalized mean squared dataset			
55.4159	51.3323	48.4346	45.8690	0.4573	0.7380	0.8295	0.7953
46.4307	53.0492	56.1401	47.7569	0.5411	0.9918	0.8701	0.7656
43.8901	48.1202	53.6939	50.2418	0.2579	0.2632	0.5319	1.0100
45.1617	50.6599	56.3062	45.6106	0.5603	0.6386	0.7012	0.5632
44.1584	55.9437	51.6196	45.7072	0.7805	0.5184	0.5676	0.5723
52.3354	55.6003	47.8481	47.4066	0.8863	0.4786	0.7742	1.0000
57.3615	51.9802	44.2522	45.0402	0.8338	0.6825	0.5801	0.5094

(1) Constructing Detector Set by Using Variable Threshold Real-Value Negative Selection Algorithms to Collect a Certain Quantity of Data

In this study, 100 samples of wind turbine gearbox positive data and two kinds of fault data are selected, and time-frequency analysis of these data samples is carried out to obtain time-frequency images.

(2) Image preprocessing

The feature vectors are taken from the three samples' time-frequency pictures. Offline training is used for the first 50 eigenvector samples. The last 50 eigenvectors are put to the test. To match the off-line trained detector set D, the vector detector E (m, s) $> R$ is employed. Each detector is individually matched. The detector is turned on when the Euclidean distance (matching distance) $E = r$.

(3) Observing the detector set, which detector is activated, determining the fault type, and finally getting the diagnosis results.

4. Discussion

(1) Data are normalized to facilitate the application of data in experiments. Table 2 shows some mean square datasets and normalized mean square datasets. The data in Table 2 comes from the data extracted by MATLAB for the vibration of the sensor on the gear.

(2) From the gray level co-occurrence matrix, extract the picture feature vector. Positive data from a wind turbine gearbox, as well as two types of fault data, are processed in this work. For each dataset, 100 samples are chosen. The time-frequency analysis of these data samples yields time-frequency images. In order to extract visual features, a gray level co-occurrence matrix and Hu invariant moments are used. The gray level co-occurrence matrix of each image in four offset directions is calculated separately. After fusion by weighting method, an improved gray level co-occurrence matrix is obtained. The extracted features of the gray level co-occurrence matrix are worth getting the image feature vectors of three different states of the gear and normalizing them. The results are as shown in Table 3.

By counting 300 samples based on GLCM eigenvector, Hu moment invariant eigenvector and GLCM-Hu eigenvector, the diagnosis results are shown in Figure 4.

In normal state, tooth surface wear state, and gear broken state, the diagnostic accuracy of image feature vectors extracted by GLCM is 83%, 78%, and 80%, respectively; the diagnostic accuracy based on Hu invariant moment extraction is 86%, 76%, and 82%, and the feature vectors extracted by LCM-Hu fusion are 90%, 91%, and 94%. The results show that the fusion of gray level co-occurrence matrix and Hu

Table 3: GLCM feature vector.

Characteristic parameters	T_1	T_2	T_3	T_4
Normal status	0.263	0.971	−1.401	0.178
Gear broken state	0.352	0.761	−1.462	0.337
Tooth surface wear state	0.504	−1.479	0.235	0.722

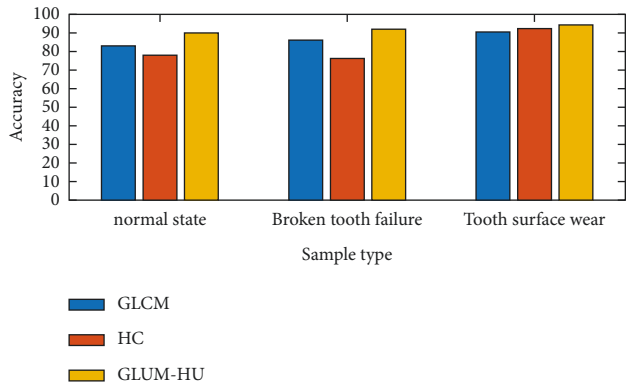

Figure 4: Diagnostic result statistics.

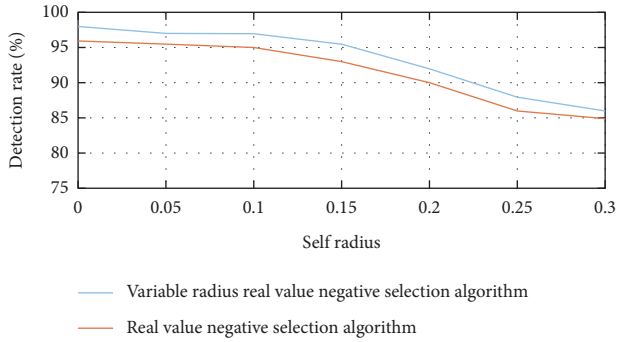

Figure 5: The relationship chart between of self-radius and detection rate.

invariant moment extract features can significantly improve the accuracy.

(3) The real negative selection algorithm with variable radius is used for fault diagnosis. Figures 5 and 6 are the contrast diagrams of the detection rate and the number of detectors under different radii of the self-body by the improved variable radius

From Figure 6, we can see that the detection rate of the detector decreases as the self-radius increases, because the large radius of the self covers the individual elements of the non-self-set. The detection rate of the improved algorithm training detector is higher than that of the original algorithm training detector, and the black hole range is effectively controlled. With the increase of the autologous radius, a smaller radius detector is needed to cover the nonautologous region, so the number of detectors required increases.

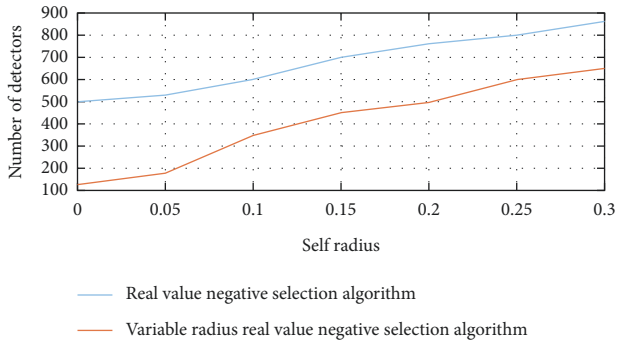

Figure 6: The relationship chart between self-radius and detector number.

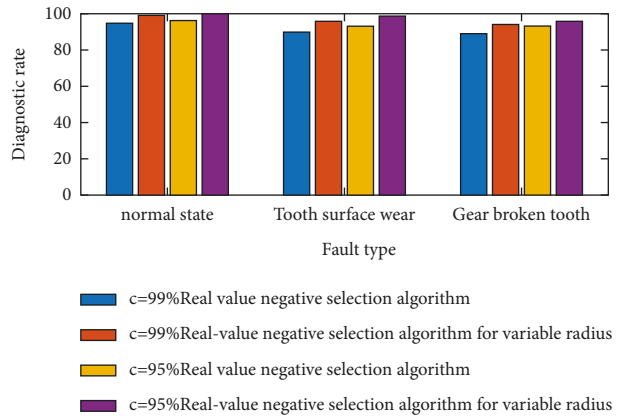

Figure 7: The diagnostic rate contrast between improved V-detector and original V-detector.

In order to compare the results of fault diagnosis based on improved variable radius real-value negative selection algorithm and original algorithm, self-radius $r_{self} = 0.1$, coverage rate $c = 95\%$, and $c = 99\%$ are set in the simulation experiment. The number of detectors generated is 375 and 613. The number of detectors generated by the improved variable radius real negative selection algorithm was 281 and 396, and the test was repeated 20 times. From the data in Figure 7, it can be seen that the diagnostic rate increases with the increase in coverage.

5. Conclusions

The correlation between eigenvalues is employed to fuse eigenvalues in this work, and vibration signals gathered from gearboxes in wind power transmission machinery are diagnosed under normal and fault situations. The resultant eigenvectors have improved resolution characteristics. We can observe from the experimental findings that the desired diagnostic accuracy is achieved. Simultaneously, it is demonstrated that a fault detection approach based on picture feature extraction and a real negative selection algorithm can accurately diagnose wind turbine transmission machinery, the fault diagnosis rates of the two are 98% and 93%, respectively.

Artificial immune algorithm can be deeply studied to make it have the same dynamic adaptive function as the immune system. By improving the mathematical model of AIA, setting the parameters and studying the convergence of AIA, a more stable fault diagnosis model of AIA is established.

Data Availability

The data that support the findings of this study are available from the corresponding author upon reasonable request.

Conflicts of Interest

The authors declare that they have no conflicts of interest.

Acknowledgments

This work was supported by Science and Technology Project of China Huaneng Group Co., Ltd "Optimization Research on preventing pitch system of Sinovel wind turbine from stuck".

References

[1] Y. Lei, J. Lin, Z. He, and M. J. Zuo, "A review on empirical mode decomposition in fault diagnosis of rotating machinery," *Mechanical Systems and Signal Processing*, vol. 35, no. 1-2, pp. 108–126, 2013.

[2] H. Henao, G. A. Capolino, M. Fernandez-Cabanas et al., "Trends in fault diagnosis for electrical machines: a review of diagnostic techniques," *IEEE industrial electronics magazine*, vol. 8, no. 2, pp. 31–42, 2014.

[3] F. Camci, K. Medjaher, N. Zerhouni, and P. Nectoux, "Feature evaluation for effective bearing prognostics," *Quality and Reliability Engineering International*, vol. 29, no. 4, pp. 477–486, 2013.

[4] J. Chen, J. Pan, Z. Li, Y. Zi, and X. Chen, "Generator bearing fault diagnosis for wind turbine via empirical wavelet transform using measured vibration signals," *Renewable Energy*, vol. 89, pp. 80–92, 2016.

[5] Y. Amirat, V. Choqueuse, and M. Benbouzid, "EEMD-based wind turbine bearing failure detection using the generator stator current homopolar component," *Mechanical Systems and Signal Processing*, vol. 41, no. 1-2, pp. 667–678, 2013.

[6] W. Yang, P. J. Tavner, C. J. Crabtree, Y. Feng, and Y. Qiu, "Wind turbine condition monitoring: technical and commercial challenges," *Wind Energy*, vol. 17, no. 5, pp. 673–693, 2014.

[7] Z. Li, Y. Jiang, C. Hu, and Z. Peng, "Recent progress on decoupling diagnosis of hybrid failures in gear transmission systems using vibration sensor signal: a review," *Measurement*, vol. 90, pp. 4–19, 2016.

[8] V. C. M. N. Leite, J. G. Borges da Silva, G. F. C. Veloso et al., "Detection of localized bearing faults in induction machines by spectral kurtosis and envelope analysis of stator current," *IEEE Transactions on Industrial Electronics*, vol. 62, no. 3, pp. 1855–1865, 2015.

[9] C. Li and M. Liang, "Time–frequency signal analysis for gearbox fault diagnosis using a generalized synchrosqueezing transform," *Mechanical Systems and Signal Processing*, vol. 26, pp. 205–217, 2012.

[10] J. Cheng, Y. Yang, and Y. Yang, "A rotating machinery fault diagnosis method based on local mean decomposition," *Digital Signal Processing*, vol. 22, no. 2, pp. 356–366, 2012.

[11] L. F. Villa, A. Reñones, J. R. Perán, and L. J. de Miguel, "Statistical fault diagnosis based on vibration analysis for gear test-bench under non-stationary conditions of speed and load," *Mechanical Systems and Signal Processing*, vol. 29, pp. 436–446, 2012.

[12] Y. Wang, R. Markert, J. Xiang, and W. Zheng, "Research on variational mode decomposition and its application in detecting rub-impact fault of the rotor system," *Mechanical Systems and Signal Processing*, vol. 60-61, pp. 243–251, 2015.

[13] A. S. Raj and N. Murali, "Early classification of bearing faults using morphological operators and fuzzy inference," *IEEE Transactions on Industrial Electronics*, vol. 60, no. 2, pp. 567–574, 2013.

[14] V. Muralidharan and V. Sugumaran, "A comparative study of Naïve Bayes classifier and Bayes net classifier for fault diagnosis of monoblock centrifugal pump using wavelet analysis," *Applied Soft Computing*, vol. 12, no. 8, pp. 2023–2029, 2012.

[15] A. M. D. Younus and B. S. Yang, "Intelligent fault diagnosis of rotating machinery using infrared thermal image," *Expert Systems with Applications*, vol. 39, no. 2, pp. 2082–2091, 2012.

[16] H. Jiang, C. Li, and H. Li, "An improved EEMD with multiwavelet packet for rotating machinery multi-fault diagnosis," *Mechanical Systems and Signal Processing*, vol. 36, no. 2, pp. 225–239, 2013.

[17] R. Yan, R. X. Gao, and X. Chen, "Wavelets for fault diagnosis of rotary machines: a review with applications," *Signal Processing*, vol. 96, pp. 1–15, 2014.

[18] D. A. Tobon-Mejia, K. Medjaher, N. Zerhouni, and G. Tripot, "A data-driven failure prognostics method based on mixture of Gaussians hidden Markov models," *IEEE Transactions on Reliability*, vol. 61, no. 2, pp. 491–503, 2012.

[19] W. He, Y. Zi, B. Chen, F. Wu, and Z. He, "Automatic fault feature extraction of mechanical anomaly on induction motor bearing using ensemble super-wavelet transform," *Mechanical Systems and Signal Processing*, vol. 54-55, pp. 457–480, 2015.

[20] Z. Li, X. Yan, Z. Tian, C. Yuan, Z. Peng, and L. Li, "Blind vibration component separation and nonlinear feature extraction applied to the nonstationary vibration signals for the gearbox multi-fault diagnosis," *Measurement*, vol. 46, no. 1, pp. 259–271, 2013.